where

$Lo = 2.443 \times 10^{-8} v^2 k^{-2}$ the Lorenz constant
T = temperature in Kelvin

The experimental results for iron shown in Fig. 3 illustrate the characteristic decrease in thermal conductivity with increasing temperature, typical of an electrical conductor. On the other hand, the iron aluminides act more like insulators and show increased thermal conductivity as a function of temperature. At lower temperatures the electrical conductivity of iron aluminide has an electrical conductivity between metals with $10^{23}/cm^3$ conduction electrons and semimetals like As with $10^{21}/cm^3$. However, the thermal conductivity of iron and iron aluminide is only an order of magnitude apart, whereas, for insulators like sulfur with $10^{13}/cm^3$ conduction electrons, it is 10 orders of magnitude lower in electrical conductivity than iron aluminide. This results from an increase in the number of conducting electrons available for energy transfer at the higher temperatures. Figure 3 indicates that compositional differences near stoichiometric Fe_3Al have little effect on the thermal conductivity as a function of temperature.

The accuracy in the thermal conductivity determination depends on the accuracy of the temperature as well as the accuracy and stability of the voltage and current measurements. Electrical resistance and thermal conductivity data for iron showed Curie transformations at 1043 K.[4] Similar results were reported by Smithells.[5] The temperature control was ± 1°C, and the temperature profile was reasonably uniform. Accuracy of the experimental resistance measurements was $10^{-4}/cm^2$.

Unfortunately, this sensitivity is inadequate to detect the order/disorder transitions in iron aluminide. The samples were 50-mm iron aluminide rectangular bars with a 10-to-1 aspect ratio. According to Vennegues et al.[6] an aspect ratio greater than 100-to-1 is necessary to observe the resistivity changes due to the order/disorder transformations. Larger temperature steps are also necessary due to the strong magnetic effects associated with spin disorder scattering and electronic structure effects. Nevertheless, the experimental results are consistent with the recommended iron thermal conductivity data from Ho et al.[4] shown in Fig. 3. They compiled 75 papers reporting iron thermal conductivity data.

Conclusions

1) Compositional differences had little effect on the thermal conductivity of iron aluminide alloys in the region of Fe_3Al ($Fe_{77}Al_{23}$, $Fe_{73}Al_{27}$, and $Fe_{26}Al_{24}$).

2) Thermal conductivities of iron aluminide alloys in the region of Fe_3Al increase linearly as a function of temperature.

3) Electrical resistivity measurements for iron used in thermal conductivity calculations are in agreement with available literature values.

References

[1]Ashcroft, N. W., and Mermin, N. D., *Solid State Physics*, Holt, Rinehart and Winston, Philadelphia, PA, 1976, p. 22.

[2]Sutton, W. H., "Apparatus for Measuring Thermal Conductivity of Ceramic and Metallic Materials to 1200°C," *American Ceramic Society*, Vol. 43, No. 2, 1960, pp. 81–87.

[3]Rossiter, P. L., "Electrical Resistivity Near the Critical Point in Binary Alloys," *Journal of Physics F: Metal Physics*, Vol. 10, No. 7, 1980, pp. 1459–1465.

[4]Ho, C. Y., Powell, R. W., and Liley, P. E., "Thermal Conductivity of the Elements," *Journal of Physical Chemical Reference Data*, Vol. 3, Supp. 1, 1974, pp. 1:366–1:337.

[5]Smithells, C. J., *Metals Reference Book*, Interscience, New York, 1955, p. 636.

[6]Vennegues, P., Cadeville, C., Pierron-Bohnes, V., and Afyouni, M., "Strong Decrease of the Activation Energy as a Function of Al Content in $FeAl_x$ Alloys ($x \leq 30$ at .%) Deduced from Kinetic Measurements of Ordering," *Acta Metallurgica et Materilia*, Vol. 38, No. 11, 1990, pp. 2199–2213.

Characterization of Thermal Performance of Fibrous Insulations Subject to a Humid Environment

K. Vafai*
Ohio State University, Columbus, Ohio 43210

Nomenclature

A = aspect ratio, $\bar{H}/\bar{L}$
$\bar{H}$ = height of the porous insulation, m
$\bar{H}'$ = length of the opening, m
$\bar{K}$ = permeability, m^2
$\bar{k}_i$ = thermal conductivity for phase i, W/m-K
$\bar{k}_{\text{eff}}$ = effective thermal conductivity, W/m-K
$\bar{L}$ = thickness of the insulation, m
Le = Lewis number, $\bar{\alpha}_{\text{eff},0}/\bar{D}_{v,\text{eff}}$
$\dot{m}$ = condensation rate
Pe = Peclet number, $\bar{v}_{\gamma,0}\bar{L}/\bar{\alpha}_{\text{eff},0}$
T = dimensionless temperature, $\bar{T}/\Delta\bar{T}$
$\bar{T}_{\infty,c}$ = cool-side ambient temperature, K
$\bar{T}_{\infty,h}$ = hot-side ambient temperature, K
ε = volume fraction
η = opening size, $\bar{H}'/\bar{H}$
ρ_i = dimensionless density for phase i, $\bar{\rho}_i/\bar{\rho}_{i,0}$
ρ_v = dimensionless vapor density, $\bar{\rho}_v/\bar{\rho}_{v,0}$

Subscripts
a = air phase
c = cool side
eff = effective properties
h = hot side
i = ith phase
s = saturation quantities
v = vapor phase
β = liquid phase
γ = gas phase
σ = solid matrix
∞ = ambient
0 = reference quantities

Superscript
- = dimensional quantities

Introduction

IN this work the insulating capability of a typical Fiberglas® insulation slab is evaluated when it is exposed to different types of environment on each side of the slab. The investigation is based on the theoretical work that takes heat conduction, natural convection, phase change, and gas infiltration into account. The results are analyzed and combined with the latest theoretical work and useful heat transfer characteristics are found for each of the materials studied. Various curves for the heat flux are obtained in which several pertinent parameters are varied and their effects on the heat transfer behavior are observed. These parameters include the humidity, temperature, and pressure differences across the insulation, the thickness of the insulation matrix, and the opening sizes and their respective locations. It is shown that the moisture within the material and the gas infiltration significantly

Received Sept. 3, 1991; revision received Feb. 28, 1992; accepted for publication March 2, 1992.

*Professor of Mechanical Engineering, Department of Mechanical Engineering. Member AIAA.

increase the heat flux across the insulation slab. For example, in buildings where an insulating material is subjected to a humid environment, the heat transfer rate through the insulation matrix will significantly increase. This fact was confirmed by Perrine[1] who had experimentally shown that the presence of liquid water and water vapor in the insulation matrix enhances the heat transfer. The presence of moisture is caused either by condensation of the infiltrated water vapor or simply by leakage on rainy days. It is illustrated that the insulation's thermal conductivity has a minor effect on the heat transfer behavior.

Tien and Vafai[2,3] used the governing energy equation, liquid and gas phases equations of motion, liquid and gas phases continuity equations, gas phase diffusion equation, and the pertinent thermodynamic relations to analyze the problem of multiphase transport through the porous insulation slab. In this work an effort was made to abridge the gap between the available literature concerning the heat transfer through insulating matrices and the needs of the industry. Based on the results presented in this work, a clearer picture is developed for the behavior of the insulating material under different ambient conditions. The resulting conclusions can be used in improving the design and quality of the existing insulation products. This work also sets some of the guidelines for the location of the openings for removal of the trapped moisture.

Theory

As mentioned earlier, the governing equations used in investigating the heat and mass transfer in the insulation matrix are based on the work of Tien and Vafai.[2,3] Their analysis was based on a set of complicated and highly nonlinear, partial differential equations and boundary conditions which were derived through applying the local volume averaging technique to the governing balance equations and the related boundary conditions for each phase. This resulted in a set of governing equations—the energy equation, liquid and gas phase equations of motion, continuity equations for the liquid and gas phases, diffusion equation for the gas phase, plus a set of thermodynamic relationships and the volume constraint equation—which were then analyzed in detail. In Tien and Vafai[2,3] a modified Nusselt number at the hot side was defined as

$$Nu_h = \frac{1}{\eta A} \frac{\int_y^{y+\eta A} \left(-P_{19} \frac{\partial T}{\partial x} + P_3 P_4 Pe \rho_\gamma v_{\gamma x} T + P_1 P_2 \psi_\varepsilon v_{\beta x} T \right)\Big|_{x=0} dy}{P_{19}(T_{\infty,h} - T_{\infty,c}) + P_3 P_4 Pe \rho^*_\gamma v^*_{\gamma x} T_{\infty,h}} \tag{1}$$

In the above expression, A represents the aspect ratio, $\bar{H}/\bar{L}$, while $\eta = \bar{H}'/\bar{H}$ represents the opening size, P_{19}, P_3, and P_4 represent the dimensionless forms for the effective thermal conductivity, heat capacity, and density of the gas, $T_{\infty,h}$ is the temperature at the hot side of the insulation, whereas $T_{\infty,c}$ is the temperature at the cold side, ρ^*_γ and $v^*_{\gamma x}$ are dimensionless reference values for the density, and v_γ and v_β are the dimensionless gas and liquid velocities. The main variables of interest are the temperature T, the liquid volume fraction ε_β, the vapor density ρ_v, the gas density ρ_γ, the gas volume fraction ε_γ, and the condensation rate $\dot{m}$. The dimensionless variables and nondimensional parameters Pe, Le, ψ_ε, and P_j are defined in detail in Tien and Vafai.[2] The reference density of the gas embodied in P_4 is determined using

$$\bar{\rho}_{\gamma,0} = \bar{\rho}_{v,0} + \bar{\rho}_{a,0} \tag{2}$$

while the reference heat capacity of the gas embodied in P_3 is determined using

$$\bar{c}_\gamma = \frac{\bar{\rho}_v \bar{c}_v + \bar{c}_a \bar{\rho}_a}{\bar{\rho}_\gamma} \tag{3}$$

In Eq. (3) $\bar{\rho}_v$ is the local volume average density of the vapor. For a certain time level $\bar{\rho}_v$ is computed by averaging the values from the density distributions figures computed in Tien and Vafai.[2]

The quantity in the numerator of Eq. (1) represents the actual heat transfer rate through the insulation, while the quantity in the denominator represents a reference heat transfer rate, thus the Nusselt number can be written as

$$Nu_h = (Q^*/Q_0) \tag{4}$$

where Q^* is the actual dimensionless heat transfer.

Solution Methodology

Tien and Vafai,[2,3] considered four representative opening locations shown in Fig. 1 of their work. It should be noted that it is necessary to create openings in order to eliminate the trapped moisture despite the adverse effect on the insulating capability of the material. Using the results obtained in Tien and Vafai,[2] it was possible to calculate the heat transfer rate through various types of Fiberglas® insulations. To investigate the pressure stratification effects at the vertical boundaries the results in Tien and Vafai[3] were used. It can be seen from Eq. (1), that for a certain temperature difference across the insulation, the reference heat transfer can be computed from

$$Q_0 = \eta A[P_{19}(T_{\infty,h} - T_{\infty,c}) + P_3 P_4 Pe \rho^*_\gamma v^*_{\gamma x} T_{\infty,h}] \tag{5}$$

while the actual dimensionless heat transfer rate can be expressed as

$$Q^* = \int_y^{y+\eta A} \left(-P_{19} \frac{\partial T}{\partial x} + P_3 P_4 Pe \rho_\gamma v_{\gamma x} T + P_1 P_2 \psi_\varepsilon v_{\beta x} T \right)\Big|_{x=0} dy \tag{6}$$

Using the dimensional terms, Eq. (6) can be rewritten as

$$Q^* = \int_y^{y+\eta A} \left(\frac{\bar{k}_{\text{eff}} \bar{L}}{\bar{k}_{\text{eff},0} \Delta \bar{T}} \frac{\partial \bar{T}}{\partial \bar{x}} + \frac{\bar{\rho}_\gamma \bar{c}_\gamma \bar{v}_{\gamma x} \bar{T} \bar{L}}{\bar{k}_{\text{eff},0} \Delta \bar{T}} + \frac{\bar{\rho}_\beta \bar{c}_\beta \bar{v}_{\beta x} \bar{T} \bar{L}}{\bar{k}_{\text{eff},0} \Delta \bar{T}} \right)_{x=0} dy \tag{7}$$

By transferring $\bar{L}/\bar{k}_{\text{eff},0}\Delta\bar{T}$ to the left side of Eq. (7), it can be clearly seen that the remainder of the right side represents the actual dimensional heat transfer rate through the insulation, that is

$$Q = \frac{\bar{k}_{\text{eff},0} \Delta \bar{T}}{\bar{L}} Q^* \tag{8}$$

In this manner, the heat transfer rate was calculated for each of the cases shown in Figs. 1–5.

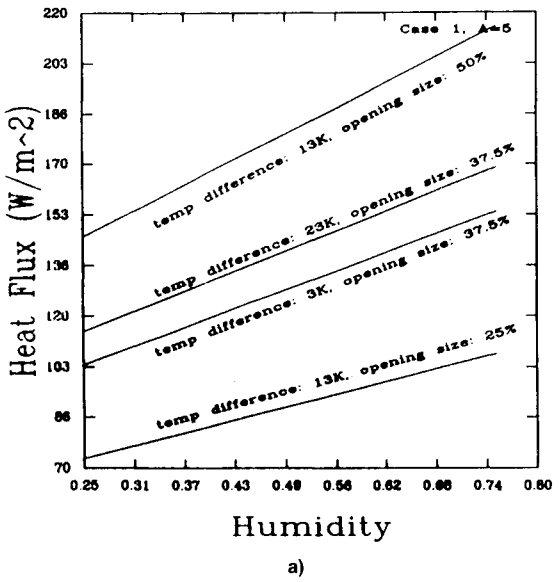

a)

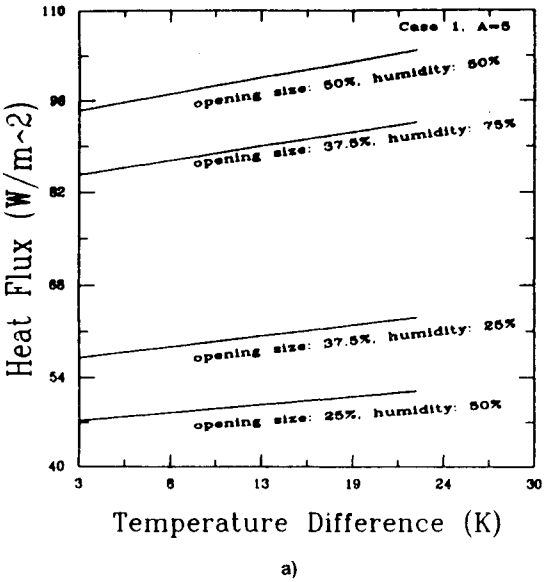

a)

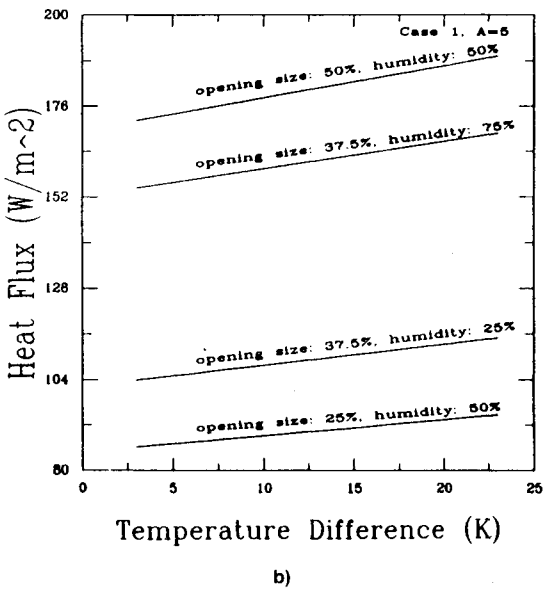

b)

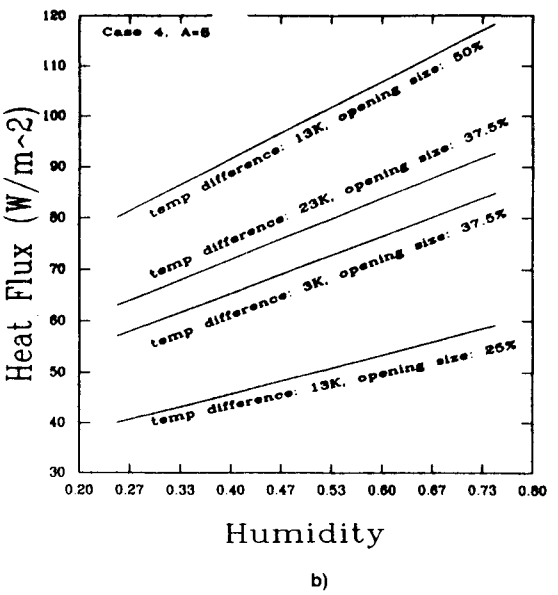

b)

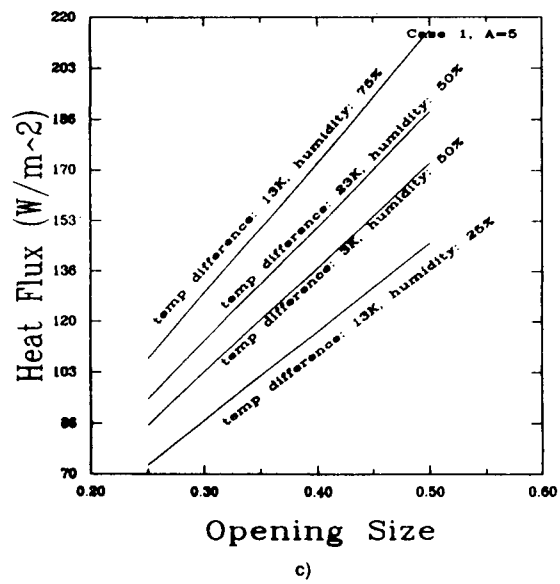

c)

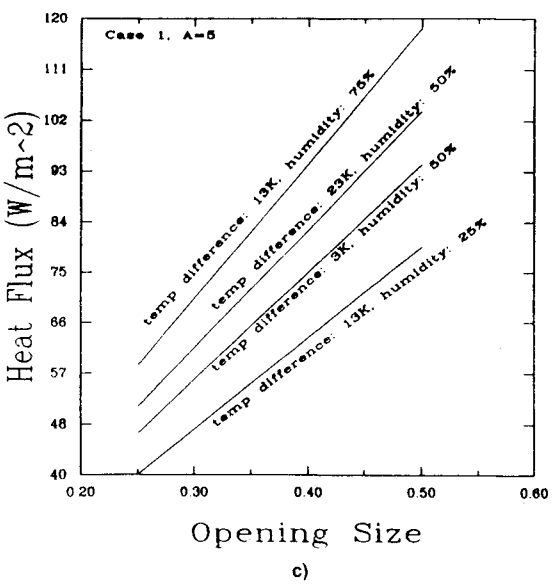

c)

Fig. 1 Heat flux variations across the insulation slab as a function of humidity, temperature difference, and opening size for case 1 and $A = 5$.

Fig. 2 Effects of the pressure stratification on the heat flux variations across the insulation slab for various parameters corresponding to Fig. 1.

Results

The heat flux through each of the following Fiberglas® materials which are frequently used in the insulation industry (Vafai and Belwafa[4]): 1) RA-24 insulation, high density wool; 2) R-11 Batt insulation, low density wool; 3) RA-22 insulation, low density board; and 4) roof deck insulation, high density board was analyzed.

The present investigation was done for the steady-state case which is of interest to the insulation industry. It should be noted that these results presented in Vafai and Tien[2,3] covered the entire transient spectrum and not just the steady state conditions. All results presented in this work are based on the analysis presented by Tien and Vafai[2] with the exception of the results presented in Fig. 2 which are based on Tien and Vafai.[3] In order to study the effects of the geometrical parameters and the ambient conditions on the insulating capability of the material, one parameter was varied while the others remained constant. This results in a set of curves for the heat transfer vs that particular parameter or ambient condition. In this work, the geometrical parameters that are of considerable interest are the opening size of the insulation, the location of the opening, and the aspect ratio while the ambient conditions are the temperatures on the hot and cold sides of the insulation, the pressure across the matrix, and the humidity. For example, in Fig. 1a for case 1 and an aspect ratio of 5, the heat flux is plotted against the humidity for various temperature differences across the insulation corresponding to different opening sizes, whereas in Figs. 1b and 1c the heat transfer was plotted against the temperature difference and the opening size respectively, for different fixed values of other pertinent parameters. The effects of pressure stratification based on the work of Tien and Vafai[3] are shown in Fig. 2. It can be clearly seen that pressure stratification, in general, results in a reduction of heat fluxes across the insulation slab.

The procedure described above was followed for cases 1, 2, and 4 discussed in Tien and Vafai.[2,3] The heat transfer behavior for case 3 was not displayed since the modified Nusselt number for this case is very similar to that in case 2. The plots for the heat flux vs temperature difference and humidity using other pertinent physical quantities as running parameters are shown in Figs. 3 and 4, respectively. In this analysis, variations in the aspect ratio were obtained by keeping the height constant while varying the thickness of the insulation slab. Comparison of Figs. 3a and 4a with Figs. 1b and 1a clearly show that the heat flux across the insulation increases with an increase in the aspect ratio. Finally, in Figs. 5a and 5b, a comparison is drawn between the heat transfer behavior for RA-24 insulation and that of R-11 Batt insulation. As can be seen, little difference is observed between the two insulation materials.

For each of the four cases described in Tien and Vafai,[2] it can be clearly seen that the humidity has a dominant effect on the heat transfer behavior. The plots obtained for the heat flux vs the humidity were compared with the experimental curve obtained from Langlais et al.[5] Both works show that the heat transfer increases with an increase in humidity. However, by carefully examining Fig. 1b (which represents case 1) it can be seen that a humidity increase from 25–75% would result in a heat transfer increase of approximately 47%. The same increase in humidity would increase the heat transfer by 20% in the experimental curve. This discrepancy is attributed to the infiltration effects which are taken into account in this work. Examining Figs. 5a and 5b reveals that there is little difference between heat flux values for R-11 Batt insulation—with a 30% higher thermal conductivity—and RA-24 insulation at different temperature differences. This observation enforces the dominant effects of even minute gas infiltration and phase change on the thermal characteristics of an insulation matrix. The results also clearly show that an increase in the opening size results in a drastic increase in the heat transfer rate. The aspect ratio was found to have a direct

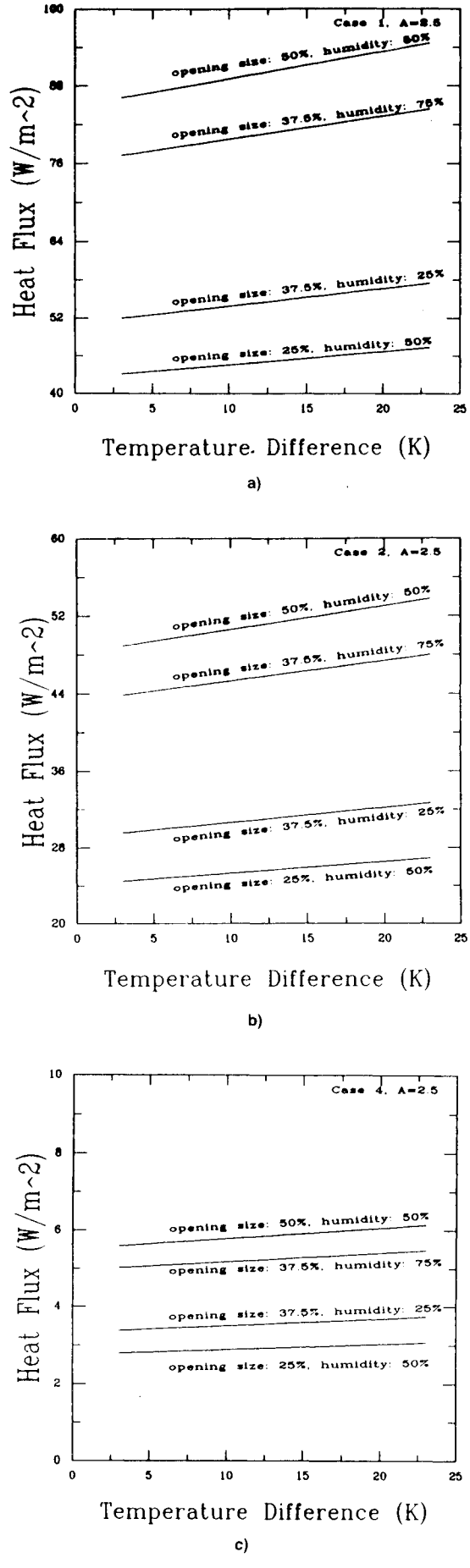

Fig. 3 Effects of humidity on heat flux variations across the insulation slab for cases 1, 2, and 4 for $A = 2.5$.

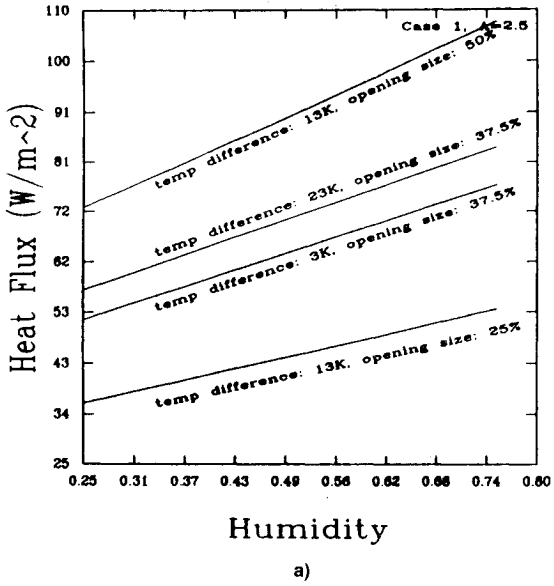

a)

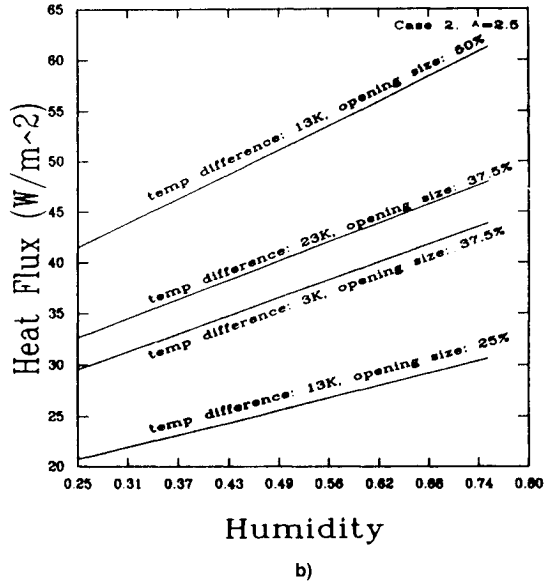

b)

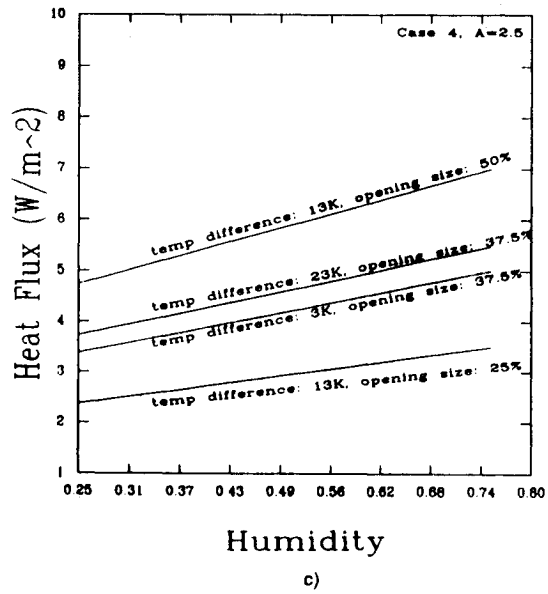

c)

Fig. 4 Heat flux variations across the insulation slab as a function of humidity for cases 1, 2, and 4 for $A = 2.5$.

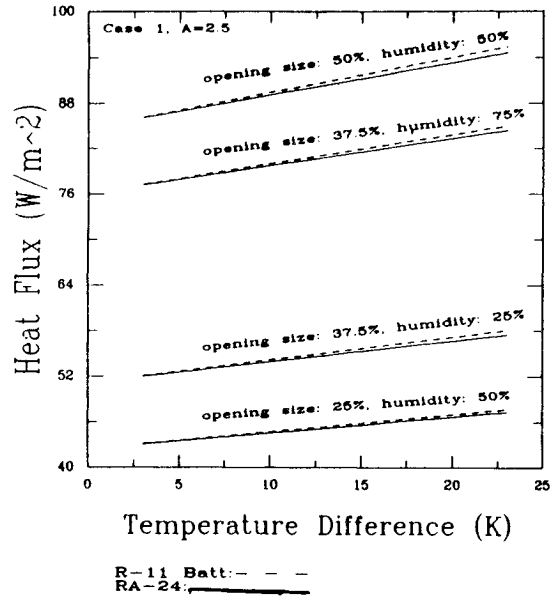

a)

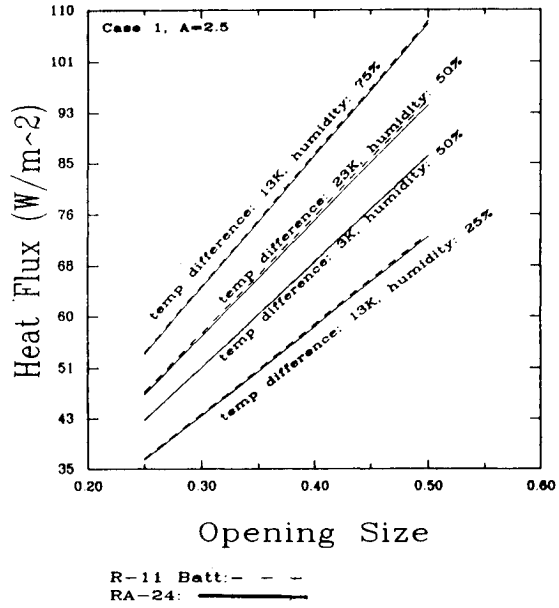

b)

Fig. 5 Comparisons between the heat transfer characteristics of RA-24 and that of R-11 Batt insulation.

effect on heat transfer across the insulation slab. Comparing Figs. 1a and 1b with Figs. 4a and 3a, it can be seen that when the aspect ratio is doubled, the heat flux is increased by approximately 100%.

The opening location has also a profound effect on the heat transfer behavior. This effect can be clearly seen when comparing the corresponding curves for the four cases with different opening locations. The proper opening location coupled with a small opening size can be selected based on the present results to obtain a reasonable insulating capability for a particular application. However, there are other factors that set the criteria for the opening size, such as the need to eliminate moisture, which if trapped in the matrix reduces the efficiency and possibly causes damage to the insulation slab. The present results can also be used to assess the effects of these other factors.

Acknowledgment

The author thanks J. Gun, R. Kort, and the Owens Corning Research Center in Granville, Ohio for providing valuable and pertinent information related to this work.

References

[1]Perrine, E. L., "Moisture Accumulation and Movements in Roof Insulation," American Society for Testing and Materials 41-53, 1982.

[2]Tien, H. C., and Vafai, K., "A Synthesis of Infiltration Effects on an Insulation Matrix," *International Journal of Heat and Mass Transfer*, Vol. 33, 1990, pp. 1263–1280.

[3]Tien, H. C., and Vafai, K., "Pressure Stratification Effects on Multiphase Transport Across a Porous Slab," *Journal of Heat Transfer*, Vol. 112, American Society of Mechanical Engineers, 1990, pp. 1023–1031.

[4]Vafai, K., and Belwafa, J., "An Experimental Investigation of Heat Transfer in Enclosures Filled or Partially Filled with a Fibrous Insulation," *Journal of Heat Transfer*, Vol. 112, American Society of Mechanical Engineers, 1990, pp. 793–797.

[5]Langlais, C., Hyrien, M., and Karlsfield, S., "Moisture Migration in Fibrous Insulating Material Under the Influence of a Thermal Gradient." *Moisture Migration in Building*, American Society for Testing and Materials STP, Vol. 779, 982, pp. 191–206.